Geochemical Perspectives Letters

The direct observation and interpretation of gas hydrate decomposition with ocean depth

L. Ma, Z. Luan, Z. Du, X. Zhang, Y. Zhang, X. Zhang

Supplementary Information

The Supplementary Information includes:

- Methods
- Supplementary Table S-1
- Supplementary Figures S-1 to S-9
- Supplementary Videos S-1 to S-4
- Supplementary Information References

Methods

Field Deployment

The experiments were conducted using the ROV Faxian on the research vessel (RV) "KEXUE" of the Institute of Oceanology, Chinese Academy of Sciences. The experiments were conducted with four pan-tilt 10× zoom HDTV cameras mounted on the ROV Faxian. The real-time temperature and pressure parameters of the surrounding seawater were obtained with a conductivity-temperature-depth (CTD, SBE 25 plus; temperature range: −5 to +35 °C, ±0.001 °C; depth limit 6800 m) sensor on the ROV. Continuous Raman spectra of the EGHs during the ascent process were acquired through a Raman insertion probe (RiP) system installed on an open tool-carrying structure mounted below the ROV Faxian. The system was controlled and communicated with via the umbilical cable of the ROV Faxian.

The RiP system included a 532 nm doubled diode-pumped Nd: YAG laser (ULA-532-100 Invictus®, KOSI), a custom-designed Raman spectrometer (N-RXNE-532-RA-SP, KOSI), and a charge-coupled device (CCD, 1024 × 256 pixel resolution, Andor Technology). The spectrometer and necessary electronic components for the communication power supply and controls were installed inside a titanium pressure chamber with a depth rating of 4500 m. A customized oil-filled optical fibre cable mounted on the outside of the titanium chamber was used to connect the Raman insertion probe for Gas hydrate (RiP-Gh) (Zhang *et al*., 2017a, 2017b). RiP-Gh is an improved new version of the deep-sea Raman insertion Probe (RiP), designed specifically for the collection of solid-translucent samples (Zhang *et al*., 2017b; Du *et al*., 2018). RiP-Gh can directly touch or insert itself into gas hydrate samples. The focal point of the laser beam was designed to enter approximately 3 mm inside the volume of each gas hydrate sample, which allowed for the removal of interference caused by the surrounding seawater from the measured Raman signal.

Experimental Field Conditions

The SCS contains numerous sizable petroliferous basins. High rates of sedimentation in the SCS facilitate the creation of natural gas hydrate formations, and the presence of complex bottom faults or diapiric structures provides ideal conditions for gas transport (Hu *et al*., 2013; Zhang *et al*., 2019, 2020). The experiment was conducted in the Haima, Lingshui, and Site F cold seep areas in the SCS. The Site F cold seep is located on the northern continental slope of the SCS, with a 1100 m water depth and 3.57 ℃ water temperature. Previous *in situ* detection studies have reported the existence of EGHs in the Site F area (Zhang *et al*., 2017a).

The Haima cold seep is located at a depth of 1509 m and has a temperature of 2.88 ℃. The Lingshui cold seep is a newly discovered vent with strong eruption characteristics at a water depth of approximately 1760 m, with a temperature of 2.56 ℃ (Table S-1). The Lingshui and Haima cold seeps are both located at the boundary of the Qiongdongnan Basin. Because of the thick organic-rich Cenozoic strata and the development of pathways for gas migration (consisting of faults and mud diapirs), the Qiongdongnan Basin is rich in natural gas hydrates (He *et al*., 2015; Fang *et al*., 2019). Notably, we investigated each cold seep vent with RiP-Gh before simulating the formation of EGHs (Fig. S-1).

Sample Preparation and *In Situ* Detection

In situ hydrate samples were formed in a cylindrical optical glass cell of approximately 9.4 L (30 cm × 20 cm, L × ⌀) in volume. The upper end of the cell was sealed with a specially made rubber gasket, which simulated natural media such as carbonate rocks and empty shells. The bottom end of the cell was exposed to the ambient seawater directly, thus creating a semi-closed space. Therefore, the cell could ensure the exchange of materials and energy between the inside and outside of the cell volume. The cell was transported to the seafloor by the ROV Faxian and was used to gather gas bubbles to simulate the formation of EGHs at different cold seeps (Video S-1). The EGHs samples were placed near the seafloor and revisited after different periods of elapsed time for *in situ* detection using Raman spectroscopy (Table S-1). The RiP-Gh probe was held by the left robotic arm of ROV Faxian, acquiring spectral information in real time during the ascent of the EGHs (Videos S-2 to S-4). We controlled the rate of uplift of the ROV in each *in situ* experiment at the same rate (Table S-1). A dissolved oxygen sensor (DOS, JFE RINKO I ARO-USB; with a temperature range of −3 to +45 ℃, ±0.02 ℃) was fastened to the frontend of the RiP-Gh probe to obtain the real-time temperature changes inside the gas hydrate. The DOS was placed at the same horizontal position as the RiP-Gh device to detect the temperature inside the EGHs.

In situ Raman Spectroscopy Data Analysis

GRAM/Al (Thermo Fisher Scientific, Inc., Waltham, USA) software was used to process the Raman spectra from the *in situ* experiments. The two apparent Raman peaks in the EGHs samples collected from the Haima and Lingshui cold seeps can be deconvoluted by performing three Gaussian fitting procedures. The three vibrational modes of methane are the $5^{12}6^2$ large cage vibration (2905 cm^{-1}), the 5^{12} small cage vibration (2915 cm^{-1}), and the gaseous CH_4 vibration (2917 cm^{-1}) (Hester *et al*., 2007; Du *et al*., 2018). There was no water peak observed in the Raman spectra of the Haima and Lingshui EGHs samples, so the dissolved CH_4 ν_1 mode (2912 cm^{-1}) was not considered in the Gaussian fit. However, the Raman spectra at Site F did show an obvious water peak, and the presence of dissolved phase methane was considered (Fig. S-2).

Supplementary Table

Table S-1 Parameters for the *in situ* Experiments.

Location	Depth (m)	Pressure (MPa)	Stationary period in the seafloor (h)	Temperature (°C)	pH	ROV rising rate (m/s)
Haima	1509	15.22	0.5	2.88	-	0.61
Lingshui	1760	17.76	2.6	2.56	7.97	0.63
Site F	1100	11.09	48	3.57	7.69	0.61

Supplementary Figures

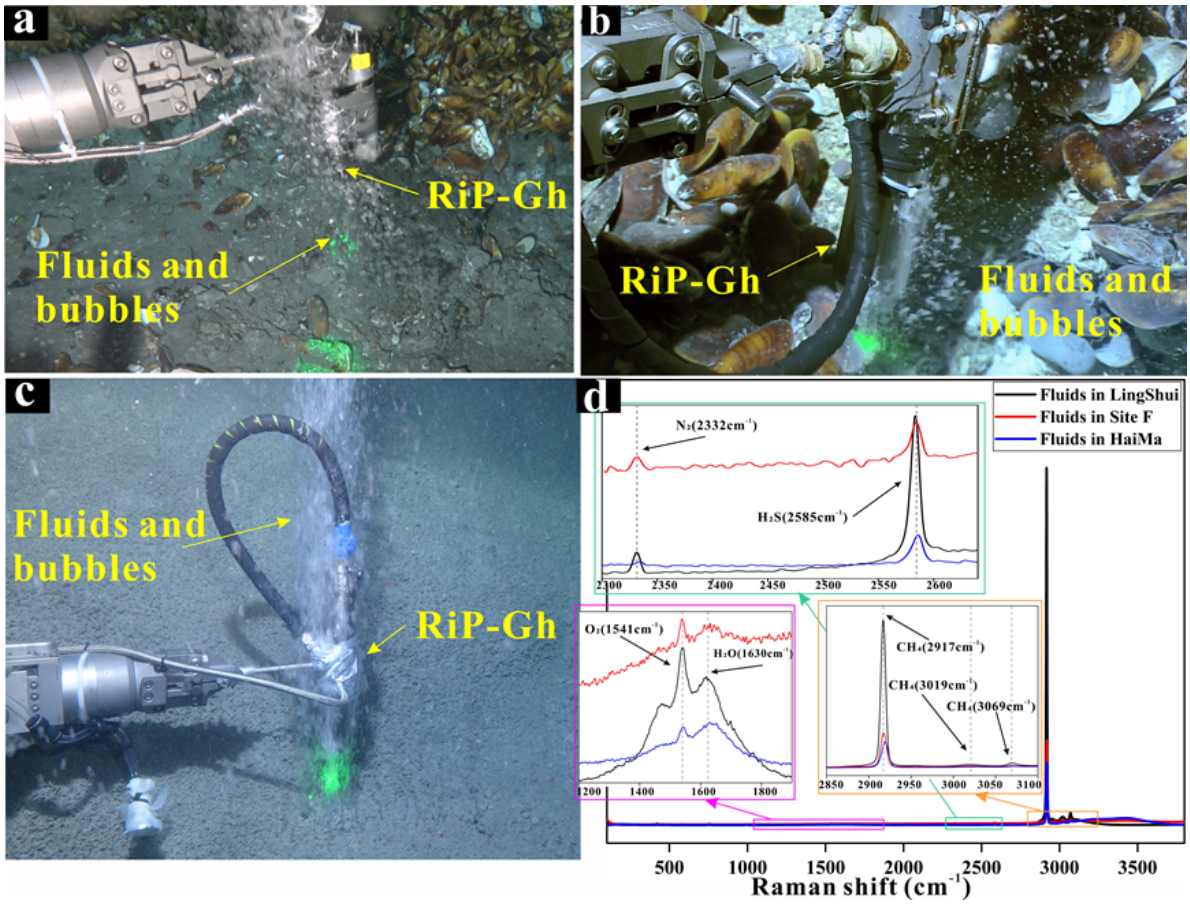

Figure S-1 Insert *in situ* detection of fluids and bubbles erupted from **(a)** Haima, **(b)** Site F and **(c)** Lingshui cold seep vent using RiP-Gh system. **(d)** *In situ* Raman spectra of different cold seep vent.

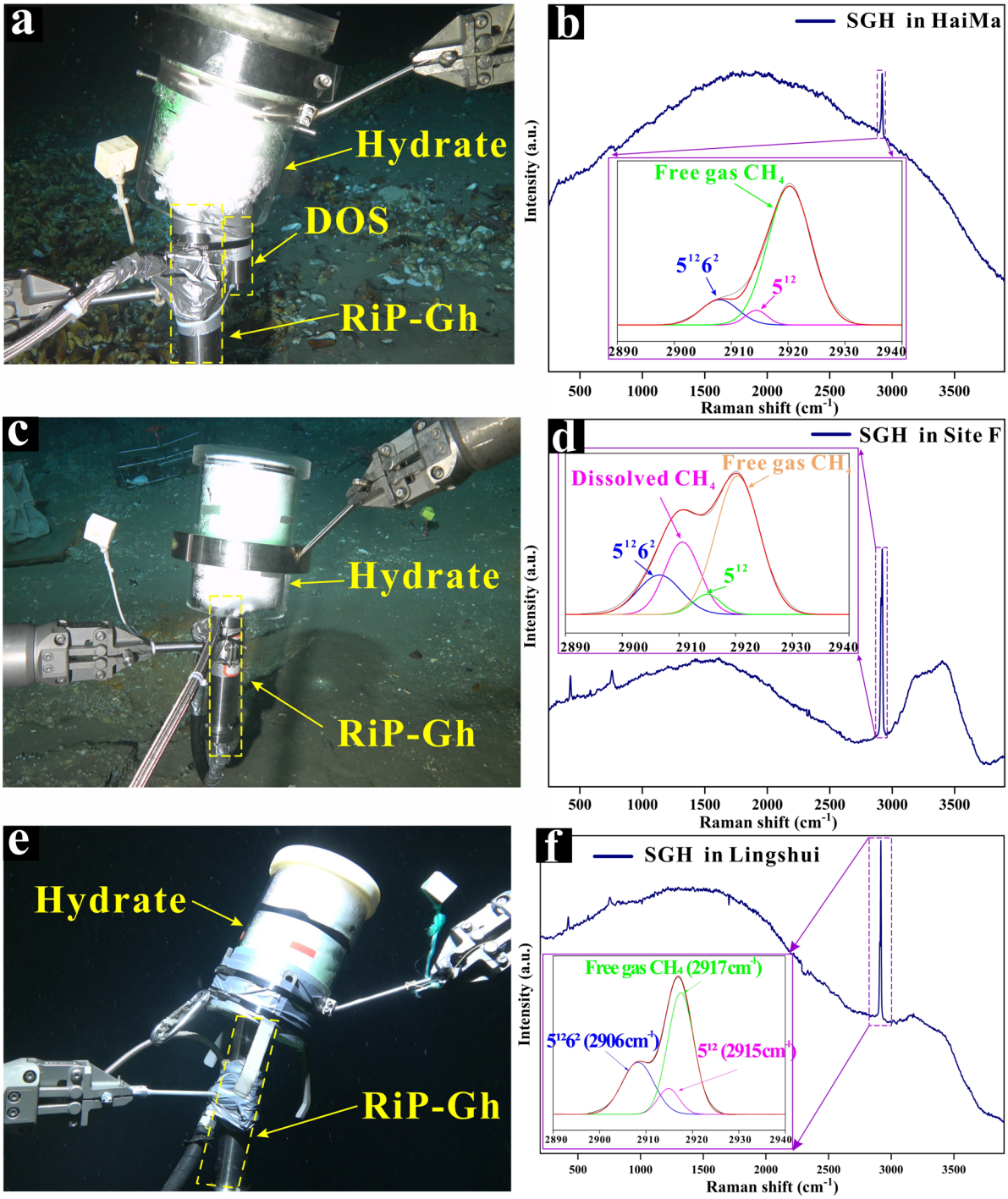

Figure S-2 Fluids and gas bubbles gathered to form the exposed hydrates for in situ detection in **(a)** Haima, **(c)** Site F and **(e)** Lingshui. **(b, d, f)** *In situ* Raman spectroscopy and the deconvolution with Gaussian fit conducted to the two Raman peaks in different cold seep areas.

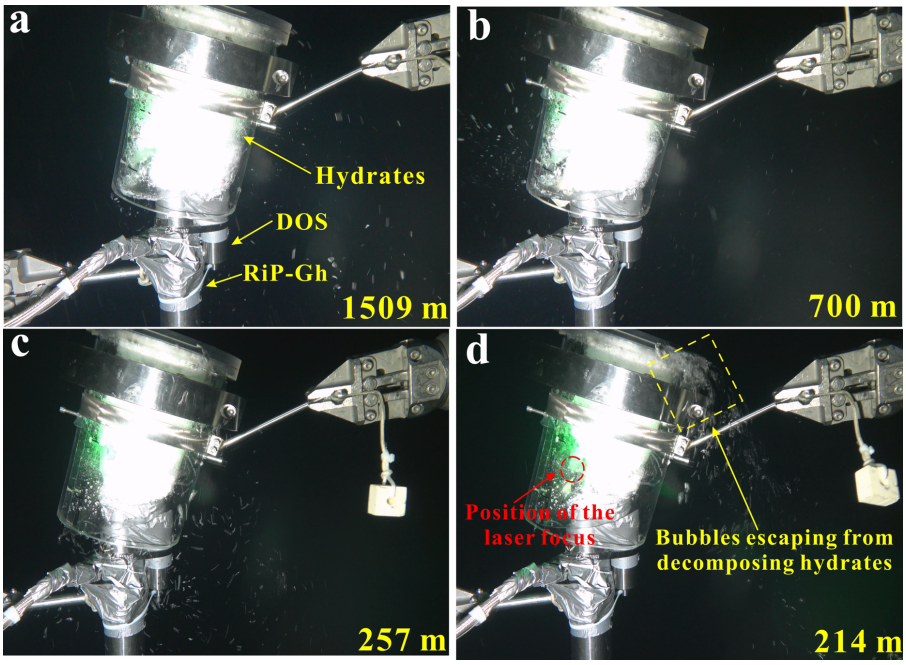

Figure S-3 Images showing hydrate collection and monitoring controlled by the ROV manipulator in Haima *in situ* experiment.

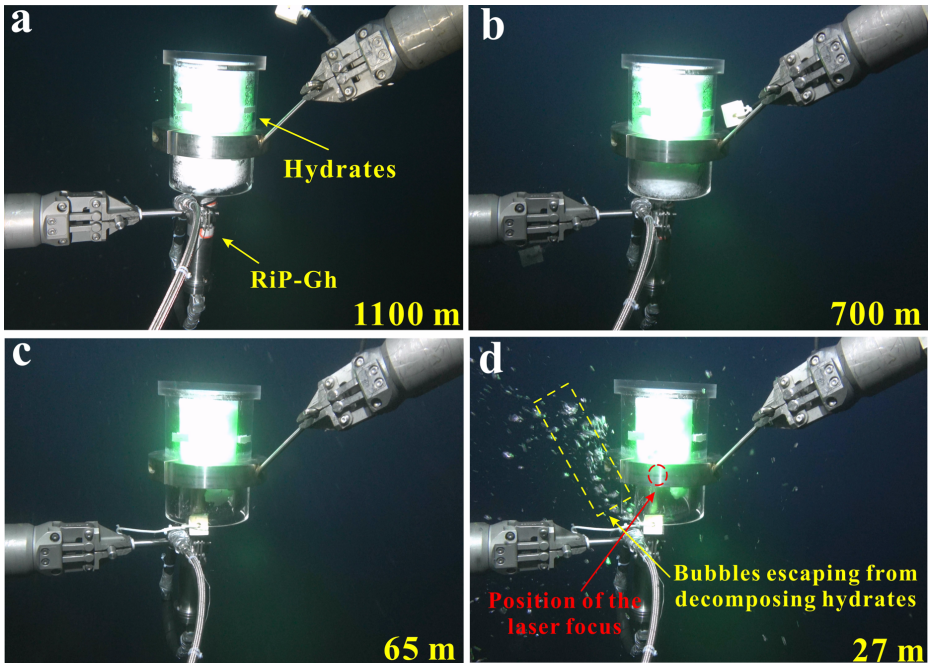

Figure S-4 Images showing hydrate collection and monitoring controlled by the ROV manipulator in Site F *in situ* experiment.

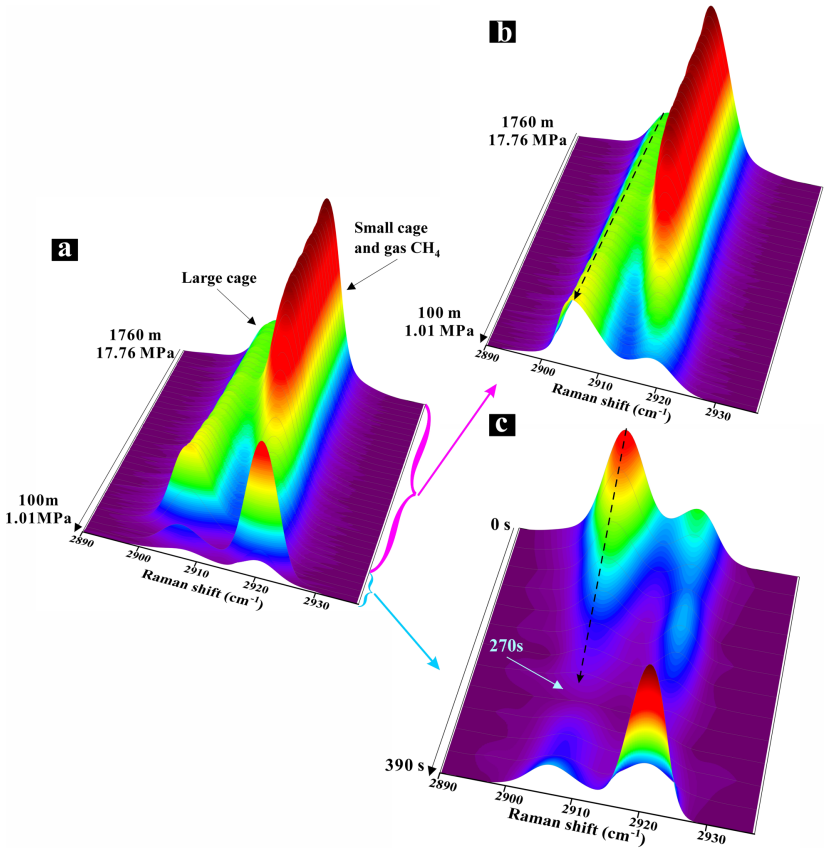

Figure S-5 *In situ* Raman spectra for hydrate samples during ROV uplift in Lingshui. **(a)** ROV overall uplift process, 17.76–1.01 MPa (1760–100 m). **(b)** The stage of continuous growth of 2907 cm^{-1} Raman intensity and continuous decrease of 2917 cm^{-1} Raman intensity. **(c)** Hydrate decomposition stage at the probe starts.

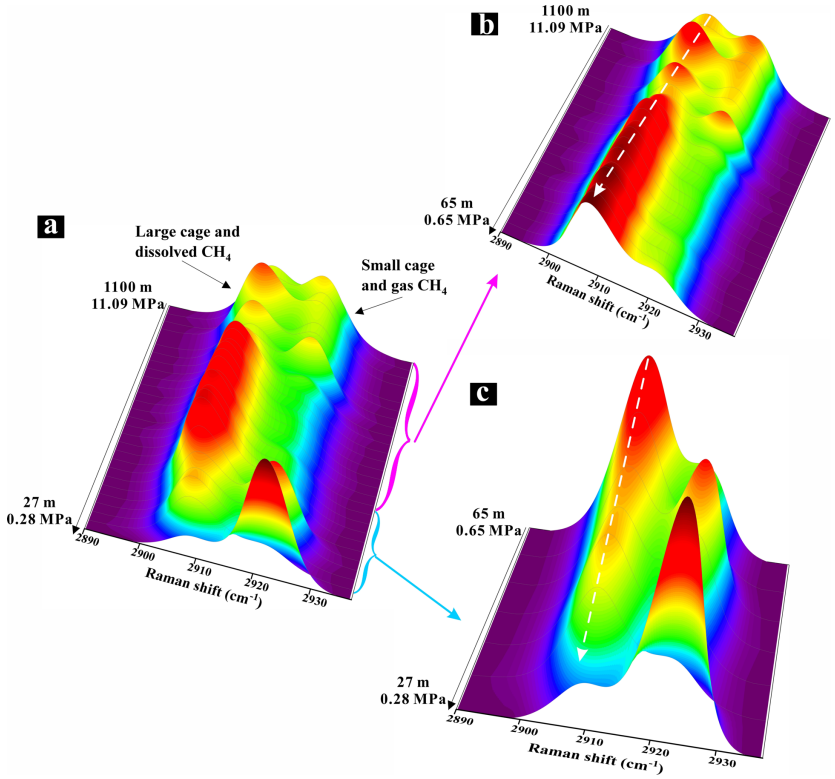

Figure S-6 *In situ* Raman spectra for hydrate samples during ROV uplift in Site F. **(a)** ROV overall uplift process, 11.09–0.28 MPa (1100–27 m). **(b)** The stage of continuous growth of 2907 cm^{-1} Raman intensity and continuous decrease of 2917 cm^{-1} Raman intensity. **(c)** Hydrate decomposition stage at the probe starts.

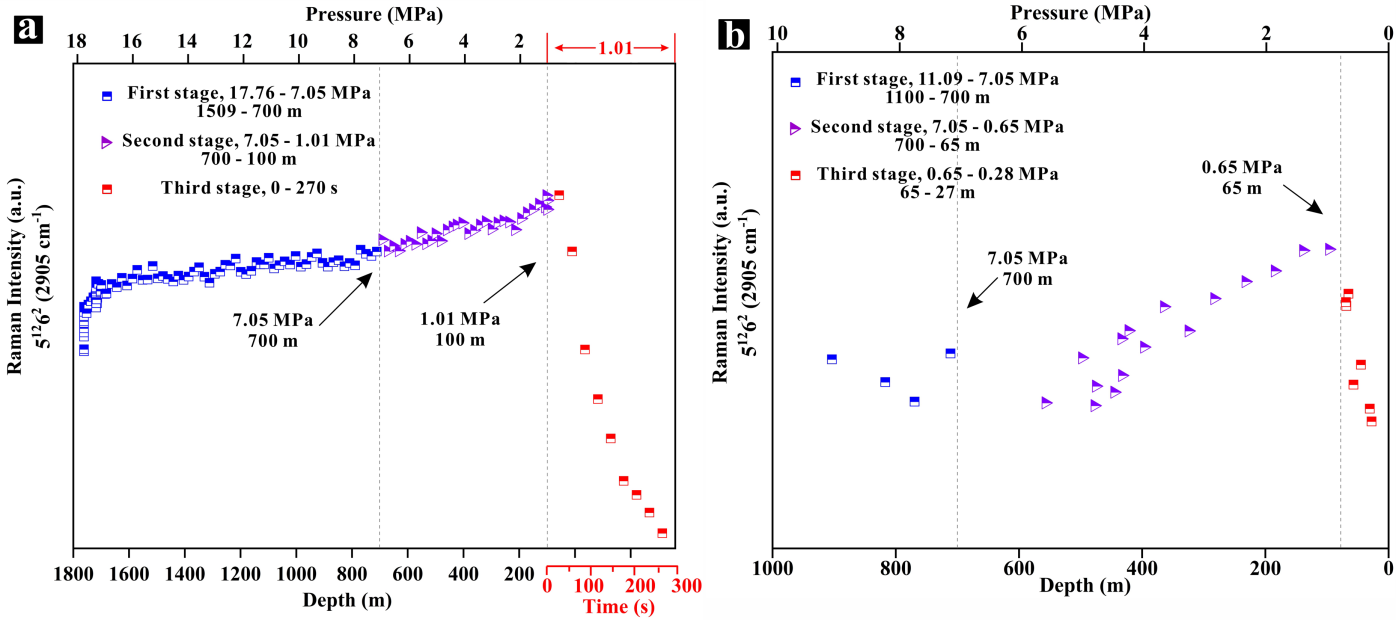

Figure S-7 Variation of large cage Raman intensity with pressure during hydrate uplift in **(a)** Lingshui and **(b)** Site F.

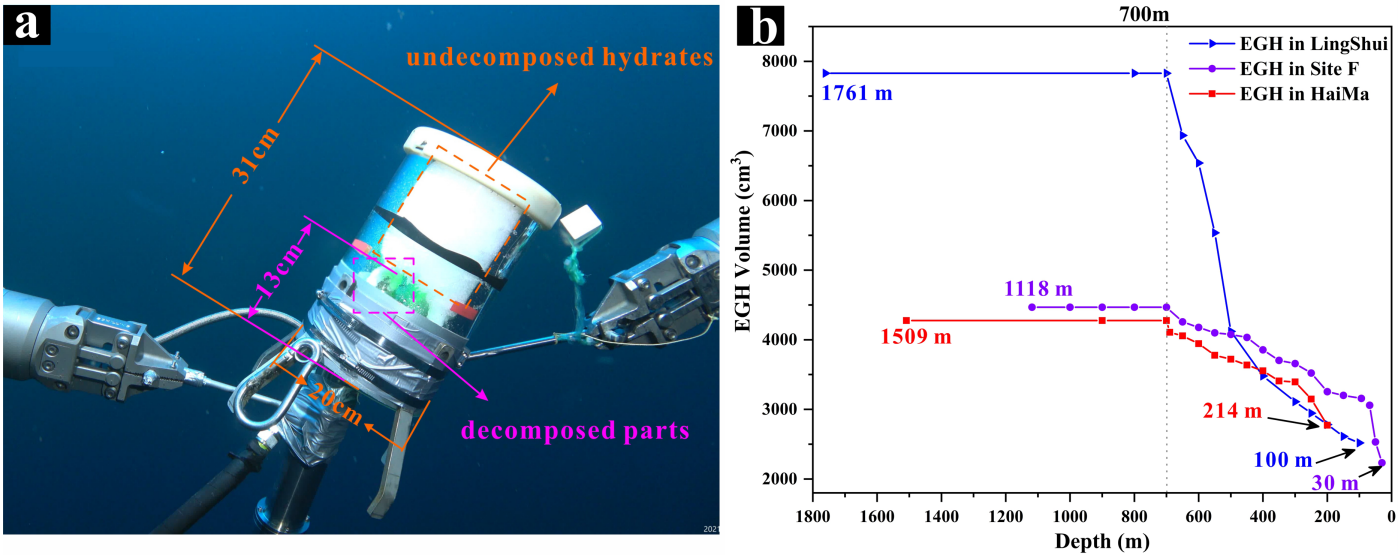

Figure S-8 **(a)** Schematic of EGHs volume estimation. **(b)** Volume variation of EGH with depth during the *in situ* experiments in the Haima cold seep area (the red line), Lingshui cold seep area (the blue line), and Site F cold seep area (the purple line).

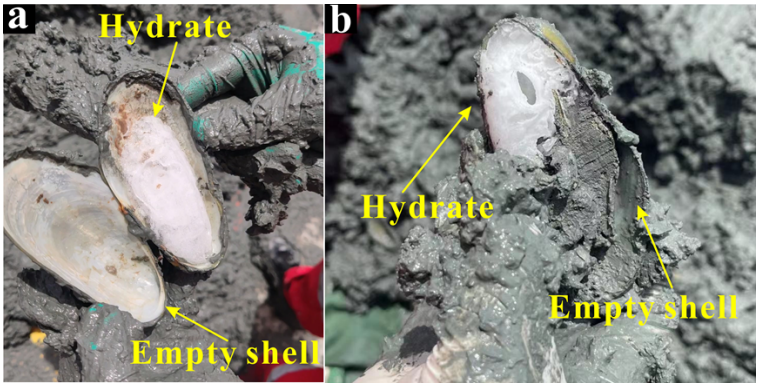

Figure S-9 Exposed gas hydrates formed in empty shells on the seafloor (Haima cold seep area).

Supplementary Videos

The video material provided for this study have all been accelerated.

Video S-1 The formation of EGHs in the Haima, Lingshui, and Site F cold seep area in South China Sea.
Video S-2 *In situ* experiments on the rise process of EGHs in the Haima cold seep area.
Video S-3 *In situ* experiments on the rise process of EGHs in the Lingshui cold seep area.
Video S-4 *In situ* experiments on the rise process of EGHs in the Site F cold seep area.

Videos S-1 through S-4 (.mp4) are available for download from the online version of this article at https://doi.org/10.7185/geochemlet.2327.

Supplementary Information References

Du, Z., Zhang, X., Xi, S., Li, L., Luan, Z., Lian, C., Wang, B., Yan, J. (2018). *In situ* Raman spectroscopy study of synthetic gas hydrate formed by cold seep flow in the South China Sea. *Journal of Asian Earth Sciences* 168, 197–206. https://doi.org/10.1016/j.jseaes.2018.02.003

Fang, Y., Wei, J., Lu, H., Liang, J., Lu, J., Fu, J., Cao, J. (2019) Chemical and structural characteristics of gas hydrates from the Haima cold seeps in the Qiongdongnan Basin of the South China Sea. *Journal of Asian Earth Sciences* 182, 103924. https://doi.org/10.1016/j.jseaes.2019.103924

Hester, K.C., Dunk, R.M., White, S.N., Brewer, P.G., Peltzer, E.T., Sloan, E.D. (2007) Gas hydrate measurements at Hydrate Ridge using Raman spectroscopy. *Geochimica et Cosmochimica Acta* 71, 2947–2959. https://doi.org/10.1016/j.gca.2007.03.032

He, J., Su, P., Lu, Z., Zhang, W., Liu, Z., Li, X. (2015) Prediction of gas sources of natural gas hydrate in the Qiongdongnan Basin, northern South China Sea, and its migration, accumulation and reservoir formation pattern. *Natural Gas Industry* 35, 19–29.

Hu, B., Wang, L., Yan, W., Liu, S., Cai, D., Zhang, G., Zhong, K., Pei, J., Sun, B. (2013) The tectonic evolution of the Qiongdongnan Basin in the northern margin of the South China Sea. *Journal of Asian Earth Sciences* 77, 163–182. https://doi.org/10.1016/j.jseaes.2013.08.022

Zhang, W., Liang, J., Su, P., Wei, J., Gong, Y., Lin, L., Liang, J., Huang, W. (2019) Distribution and characteristics of mud diapirs, gas chimneys, and bottom simulating reflectors associated with hydrocarbon migration and gas hydrate accumulation in the Qiongdongnan Basin, northern slope of the South China Sea. *Geological Journal* 54, 3556–3573. https://doi.org/10.1002/gj.3351

Zhang, W., Liang, J., Yang, X., Su, P., Wan, Z. (2020) The formation mechanism of mud diapirs and gas chimneys and their relationship with natural gas hydrates: insights from the deep-water area of Qiongdongnan Basin, northern South China Sea. *International Geology Review* 62, 789–810. https://doi.org/10.1080/00206814.2018.1491014

Zhang, X., Du, Z., Luan, Z., Wang, X., Xi, S., Wang, B., Li, L., Lian, C., Yan, J. (2017a) In Situ Raman Detection of Gas Hydrates Exposed on the Seafloor of the South China Sea. *Geochemistry, Geophysics, Geosystems* 18, 3700–3713. https://doi.org/10.1002/2017gc006987

Zhang, X., Du, Z., Zheng, R., Luan, Z., Qi, F., Cheng, K., Wang, B., Ye, W., Liu, X., Lian, C., Chen, C., Guo, J., Li, Y., Yan, J. (2017b) Development of a new deep-sea hybrid Raman insertion probe and its application to the geochemistry of hydrothermal vent and cold seep fluids. *Deep Sea Research Part I: Oceanographic Research Papers* 123, 1–12. https://doi.org/10.1016/j.dsr.2017.02.005